High-order solutions of three-dimensional rough-surface scattering problems at high-frequencies. II: the vector electromagnetic case

Fernando Reitich and Catalin Turc

School of Mathematics, University of Minnesota, Minneapolis, 55455, USA

E-mail: reitich@math.umn.edu, turc@math.umn.edu

Abstract. We introduce a new numerical scheme for three-dimensional electromagnetic rough-surface scattering simulations with the capability of delivering very accurate results from low to high frequencies at a cost that is independent of the wavelength of radiation. The method is an extension of the ideas and techniques introduced in the first paper of this series [Waves Random Media, to appear] to the vector electromagnetic case, and it is based on the solution of an integral equation formulation of the scattering problem. As in the scalar case, the solution of the integral equation (i.e. the current) is expressed as a slow modulation of an oscillatory exponential of *known* phase, and explicit recursive formulas are derived for the successive terms in a series expansion of the slow envelope in inverse powers of the wavenumber. As we show, and in spite of the considerably more involved nature of the derivations and resulting formulas, the performance of the method retains the favorable characteristics that were demonstrated in the treatment of acoustic scattering problems. In particular, results with full double-precision accuracy are presented for various geometries, incidences and polarizations.

Submitted to: *Waves Random Media*

1. Introduction

The difficulties associated with the rigorous numerical prediction of the electromagnetic fields scattered by rough surfaces stem largely from the oscillatory characteristics of waves, which demand that a number of virtual degrees of freedom be associated with each single spatial variation of these on the scale of the wavelength. These difficulties then are increasingly exarcebated with increasing frequency and, in fact, they can quickly overcome the capabilities of the most advanced computational engines. For this reason, practical simulations of rough-surface scattering at high-frequencies have consistently relied on low-order asymptotic models (e.g. the Kirchhoff approximation [1, 2] —KA—, or its next order corrections [3, 4, 5, 6]) whose solutions approximate those of Maxwell's equations in the limit of vanishing wavelength. As we have recently shown however [7] (see also [8]), the low-order nature of these approximations can translate in significant errors for configurations of interest, due to their relatively slow convergence to the exact solution as the wavelength tends to zero. In that work we also showed, in the context of scalar, acoustic scattering, that approximations of arbitrarily high-order in wavelength can be attained, and easily implemented, leading to substantial improvements over classical low-order theories. In this paper we present an extension of this approach to the treatment of the full vector electromagnetic case. As we show, this extension preserves the efficiency and accuracy characteristics demonstrated in the scalar case, which allows for the rapid evaluation of scattering amplitudes with full double-precision accuracy for a a range of geometries and incidences in all polarizations.

Following [7] the method we present is based on the solution of an integral-equation formulation of the scattering problem in the frequency domain. In the present context of electromagnetic scattering we propose a scheme that solves the Magnetic Field Integral Equation (MFIE) (see e.g. [9]) which constitutes the natural extension of Maue's integral equation [10] in the scalar case. In particular, these two integral formulations display kernels with similar characteristics which allows for the resolution of their singularity to be effected in analogous manners. The overall solution method in the electromagnetic case then can proceed largely as in the scalar instance. More precisely, to allow for efficient and accurate evaluations throughout the frequency spectrum we: 1) appeal to high-frequency asymptotics to factor the unknown surface current into a highly oscillatory exponential of *known* phase (varying in-sync with the incoming radiation), and a slow vector modulation whose variations are not enhanced with increasing frequency; 2) rely on the slowly varying character of this envelope to express it in the form of a series in inverse powers of the wavenumber; 3) apply the classical theory of oscillatory integrals (see e.g. [11]) to derive a *recurrence* for the functional coefficients in this series; and 4) utilize spectrally accurate quadratures to evaluate the recursion. As we show, and in spite of the significantly more involved form of the corresponding recursive formulas, these prescriptions result in a numerical procedure that effectively delivers high-quality predictions much as in its implementation in acoustics [7].

As explained above, our method can be considered as a high-order extension of classical low-order theories (e.g. KA to which, in fact, the scheme reduces in its lowest order form). As in these theories, our current treatment assumes that the scatter results from direct incidence and it precludes shadowing effects (e.g. step 1) above relies on the former assumption, while the latter implies that integer powers suffice in step 2)). As we indicated in [7], extensions to multiple scattering/shadowing configurations (possibly based on "geometrical shadowing functions" [12], on fractional asymptotic expansions [13] or on "localized integration" [14] strategies) are left for future consideration. Within the current context then, the rest of the paper is organized as follows: first, in §2 we introduce the relevant integral formulation which we adapt to a form that is favorable for high-frequency evaluations; the asymptotic expansions of the terms in this formulation are then presented in §3 where we also derive recursive formulas that provide approximations to the unknown current of arbitrarily high order; a numerical scheme based on this recursion is detailed in §4.1 and numerical results are presented in §4.2; finally our conclusions are summarized in §5.

2. High-frequency integral equations

We consider the problem of scattering of time harmonic electromagnetic waves from a perfectly conducting surface $\Sigma = \{\mathbf{x} = (x_1, x_2, x_3) \in \mathbb{R}^3 \,:\, x_3 = f(x_1, x_2)\}$ where f is a smooth function of the variables (x_1, x_2). The scattered fields $\mathbf{E}$ and $\mathbf{H}$ satisfy Maxwell's equations

$$\begin{aligned} &\nabla \times \mathbf{E} = \quad ik\mathbf{H}, \quad \nabla \cdot \mathbf{E} = 0 \quad \text{in } \Sigma_+, \\ &\nabla \times \mathbf{H} = -ik\mathbf{E}, \quad \nabla \cdot \mathbf{H} = 0 \quad \text{in } \Sigma_+ \\ &\mathbf{n} \times \mathbf{E} = -\mathbf{n} \times \mathbf{E}^{\text{inc}} \qquad\qquad \text{on } \Sigma \end{aligned} \tag{1}$$

where

$$\Sigma_+ = \{\mathbf{x} = (x_1, x_2, x_3) \,:\, x_3 > f(x_1, x_2)\}$$

and the incidence is given by

$$\begin{aligned} \mathbf{E}^{\text{inc}} &= \mathbf{A} e^{i\mathbf{k}\cdot\mathbf{x}} = \mathbf{A} \exp(i\alpha x_1 + i\beta x_2 - i\gamma x_3), \\ \mathbf{H}^{\text{inc}} &= \mathbf{B} e^{i\mathbf{k}\cdot\mathbf{x}} = \mathbf{B} \exp(i\alpha x_1 + i\beta x_2 - i\gamma x_3), \\ \mathbf{A} &= (A^{(1)}, A^{(2)}, A^{(3)}), \\ \mathbf{B} &= (B^{(1)}, B^{(2)}, B^{(3)}), \\ \mathbf{k} &= (\alpha, \beta, -\gamma), \ |\mathbf{k}| = k, \\ \alpha &= k \sin\psi \cos\phi, \ \beta = k \sin\psi \sin\phi, \ \gamma = k \cos\psi \end{aligned}$$

with

$$\begin{aligned} \mathbf{B} &= \frac{\mathbf{k}}{|\mathbf{k}|} \times \mathbf{A}, \\ 0 &= \mathbf{A} \cdot \mathbf{k}. \end{aligned}$$

The scattering problem (1) does not have a unique solution unless specific "radiation conditions" at infinity are imposed. As is well-known, however, the classical Silver-Müller conditions [15] are not appropriate in this context (e.g. in the simplest case when Σ is an infinite plane, the specularly reflected plane waves do not satisfy this type of requirement), and weaker versions of the radiation conditions must be imposed on the scattered fields. The general form of these conditions states that scattered waves must be "upward propagating" (see e.g. [16]); in the important case of bi-periodic surfaces, the condition simply reduces to the classical radiation conditions as expressed through the Rayleigh series [17] (see §4.1).

With the addition of the proper radiation conditions, the scattering problem (1) admits various integral equation formulations, all stemming from applications of Green's identities. In the spirit of the methodology proposed in [7], we shall use an integral equation that seeks to find the physical current on the surface Σ given by

$$\mathbf{J} = \mathbf{n} \times (\mathbf{H} + \mathbf{H}^{\text{inc}}) \quad \text{on } \Sigma \tag{4}$$

where $\mathbf{n}$ is the outward normal to Σ. The scattered fields $\mathbf{E}$ and $\mathbf{H}$, then, can be recovered form knowledge of the current via the classical Stratton-Chu formulas [18]:

$$\begin{aligned} \mathbf{E}(\mathbf{x}) &= ik \int_\Sigma \left(G_k(\mathbf{x}-\mathbf{x}')\mathbf{J}(\mathbf{x}') - \frac{1}{k^2} \nabla_{\mathbf{x}'} G_k(\mathbf{x}-\mathbf{x}') \nabla^t_{\mathbf{x}'} \cdot \mathbf{J}(\mathbf{x}') \right) d\sigma(\mathbf{x}'), \\ \mathbf{H}(\mathbf{x}) &= - \int_\Sigma \nabla_{\mathbf{x}'} G_k(\mathbf{x}-\mathbf{x}') \times \mathbf{J}(\mathbf{x}') d\sigma(\mathbf{x}') \end{aligned} \tag{5}$$

where the (outgoing) free space Green's function is given by

$$G_k(\mathbf{r}) = \frac{\exp(ik|\mathbf{r}|)}{4\pi|\mathbf{r}|}$$

and $\nabla^t_{\mathbf{x}'} \cdot$ denotes the surface divergence on Σ.

With this choice of the unknown quantity and boundary conditions, two main integral equation formulations can be derived: one is an integral equation of the first kind, typically referred to as electric field integral equation (EFIE) and the other is an integral equation of the second kind, the magnetic field integral equation (MFIE) [9]. In the present context, the weak singularity of the kernel of MFIE is preferable to the more severe Cauchy-type singularity of EFIE [9], and we shall therefore choose the former for the calculations that follow. More precisely, we shall consider the equation

$$\frac{\mathbf{J}}{2} + \mathcal{K}\mathbf{J} = \mathbf{n} \times \mathbf{H}^{\text{inc}}, \quad \mathbf{x} \in \Sigma, \tag{6}$$

where the integral operator $\mathcal{K}$ is defined as

$$(\mathcal{K}\mathbf{J})(\mathbf{x}) = \mathbf{n}(\mathbf{x}) \times \int_\Sigma \nabla_{\mathbf{x}'} G_k(\mathbf{x}-\mathbf{x}') \times \mathbf{J}(\mathbf{x}') d\sigma(\mathbf{x}'). \tag{7}$$

As it easily follows from (7), the singularity in the kernel of the MFIE (6) is no worse than that corresponding to the acoustic case. Indeed, using the tangential character of the current (4), $\mathbf{n}(\mathbf{x}') \cdot \mathbf{J}(\mathbf{x}') = 0$, the integral operator (7) can be written as

$$(\mathcal{K}\mathbf{J})(\mathbf{x}) = \int_\Sigma \left((\mathbf{n}(\mathbf{x}) - \mathbf{n}(\mathbf{x}')) \cdot \mathbf{J}(\mathbf{x}') \nabla_{\mathbf{x}'} G_k(\mathbf{x}-\mathbf{x}') + \frac{\partial G_k}{\partial \mathbf{n}(\mathbf{x})} (\mathbf{x}-\mathbf{x}') \mathbf{J}(\mathbf{x}') \right) d\sigma(\mathbf{x}')$$

and, for sufficiently smooth (twice continuously differentiable) surfaces, the kernels satisfy

$$|\mathbf{n}(\mathbf{x}) - \mathbf{n}(\mathbf{x}')| \left| \nabla_{\mathbf{x}'} \frac{e^{ikr}}{r} \right| = \mathcal{O}(r^{-1}), \quad \frac{\partial}{\partial \mathbf{n}(\mathbf{x})} \frac{e^{ikr}}{r} = \mathcal{O}(r^{-1}), \ r \to 0$$

where $r = |\mathbf{x}' - \mathbf{x}|$.

As described in [7], a main impediment in the solution of (6) at high-frequencies arises from the highly oscillatory character of both the kernel and the unknown current. A basic idea towards the resolution of this issue stems from the realization that the oscillatory behavior of the *full* integrand in (6) can be determined *a priori* by appealing to high-frequency asymptotics. More precisely, the oscillations in the current can be pre-determined from the solution of the relevant limiting eikonal model, thus leaving us to find a slowly varying envelope that modulates these rapid variations. Specifically, in the present single-scattering context, the phase of the current will coincide with that of the incoming radiation (see e.g. [3, 6, 19, 20, 21, 22, 23])

$$\mathbf{J}(\mathbf{x}, k) = \exp(i\mathbf{k} \cdot \mathbf{x})\, \mathbf{J}_{\text{slow}}(\mathbf{x}, k), \tag{8}$$

where $J_{\text{slow}}(\mathbf{x}, k)$ is such that its oscillations *do not* accentuate with increasing frequency. In terms of this new, slowly oscillatory unknown equation (6) can be written as

$$\begin{aligned} \frac{1}{2}\mathbf{J}_{\text{slow}}(\mathbf{x}, k) + \mathbf{n}(\mathbf{x}) \times \int_\Sigma \exp\left[i\mathbf{k} \cdot (\mathbf{x}' - \mathbf{x})\right] \nabla_{\mathbf{x}'} G_k(\mathbf{x} - \mathbf{x}') \times \mathbf{J}_{\text{slow}}(\mathbf{x}', k)\, d\sigma(\mathbf{x}') \\ = \mathbf{n}(\mathbf{x}) \times \mathbf{B}, \quad \mathbf{x} \in \Sigma. \end{aligned} \tag{9}$$

Clearly, the function $\mathbf{J}_{\text{slow}} = (J^{(1)}_{\text{slow}}, J^{(2)}_{\text{slow}}, J^{(3)}_{\text{slow}})$ is still tangential to Σ, so that

$$J^{(3)}_{\text{slow}}(x_1, x_2, k) = f_{x_1}(x_1, x_2) J^{(1)}_{\text{slow}}(x_1, x_2, k) + f_{x_2}(x_1, x_2) J^{(2)}_{\text{slow}}(x_1, x_2, k).$$

Using this relation we can derive a parametric formulation of the vector equation (9) in the form of two coupled scalar equations for the unknowns $J^{(1)}_{\text{slow}}$ and $J^{(2)}_{\text{slow}}$, namely

$$\begin{aligned} &\frac{J^{(1)}_{\text{slow}}(x_1, x_2, k)}{2} + \frac{1}{4\pi} \int_{\mathbf{R}^2} \Big\{ \Big[(f_{x_1'} - f_{x_1}) J^{(1)}_{\text{slow}}(x_1', x_2', k) + (f_{x_2'} - f_{x_2}) J^{(2)}_{\text{slow}}(x_1', x_2', k) \Big] (x_1' - x_1) \\ &\quad + (ikr - 1) \left[(x_1' - x_1) f_{x_1} + (x_2' - x_2) f_{x_2} + f(x_1, x_2) - f(x_1', x_2') \right] J^{(1)}_{\text{slow}}(x_1', x_2', k) \Big\} \frac{1}{r^3} \\ &\quad \times \exp\left[ikr + i\alpha(x_1' - x_1) + i\beta(x_2' - x_2) - i\gamma \left(f(x_1', x_2') - f(x_1, x_2) \right)\right] \frac{\sqrt{g'}}{\sqrt{g}}\, dx_1' dx_2' \\ &\quad = -\frac{f_{x_2} B^{(3)} + B^{(2)}}{\sqrt{g}} \end{aligned} \tag{10}$$

and

$$\begin{aligned}
&\frac{J^{(2)}_{\text{slow}}(x_1,x_2,k)}{2}+\frac{1}{4\pi}\int_{\mathbf{R}^2}\Big\{\Big[(f_{x_1'}-f_{x_1})J^{(1)}_{\text{slow}}(x_1',x_2',k)+(f_{x_2'}-f_{x_2})J^{(2)}_{\text{slow}}(x_1',x_2',k)\Big](x_2'-x_2)\\
&\quad+(ikr-1)\left[(x_1'-x_1)f_{x_1}+(x_2'-x_2)f_{x_2}+f(x_1,x_2)-f(x_1',x_2')\right]J^{(2)}_{\text{slow}}(x_1',x_2',k)\Big\}\frac{1}{r^3}\\
&\quad\times\exp\left[ikr+i\alpha(x_1'-x_1)+i\beta(x_2'-x_2)-i\gamma\left(f(x_1',x_2')-f(x_1,x_2)\right)\right]\frac{\sqrt{g'}}{\sqrt{g}}\,dx_1'dx_2'\\
&\quad=\frac{f_{x_1}B^{(3)}+B^{(1)}}{\sqrt{g}}
\end{aligned}\tag{11}$$

where

$$\begin{aligned}
f_{x_j}&=f_{x_j}(x_1,x_2)\,,\\
f_{x_j'}&=f_{x_j}(x_1',x_2')\,,\\
r\quad&=|\mathbf{x}'-\mathbf{x}|=\left[(x_1-x_1')^2+(x_2-x_2')^2+(f(x_1,x_2)-f(x_1',x_2'))^2\right]^{1/2}
\end{aligned}$$

and g and g' are the determinants of the Riemannian metric (g_{ij}) induced on Σ, that is

$$g=1+f_{x_1}(x_1,x_2)^2+f_{x_2}(x_1,x_2)^2,\quad g'=1+f_{x_1}(x_1',x_2')^2+f_{x_2}(x_1',x_2')^2.$$

As in [7], to solve equations (10) and (11) we shall rely on the slowly varying character of the unknown fields to express them in the form of power series

$$J^{(l)}_{\text{slow}}(x_1,x_2,k)=\frac{1}{\sqrt{g}}\sum_{n=0}^{\infty}\frac{\mu_n^{(l)}(x_1,x_2)}{k^n},\quad l=1,\ 2.\tag{12}$$

As we show next, the coefficients $\mu_n^{(l)}$ can be *recursively* obtained through an application of the theory of oscillatory integrals [11]. We note here that, as will be naturally confirmed in the calculations that follow (see equation (24)), the restriction to integer powers of the wavenumber in (12) is possible in the absence of shadowing [21].

3. Asymptotic expansions and the recurrence

To facilitate the explicit asymptotic expansion of the *singular* integrals in (10) and (11) we begin by transforming them into integrals of *regular* functions through a polar change of variables centered around the "target point" [7]

$$x_1'=x_1+\rho\cos\theta,\ x_2'=x_2+\rho\sin\theta.$$

With this change of variables then, equations (10) and (11) translate to

$$\begin{aligned}
\sum_{n=0}^{\infty}\frac{1}{k^n}\left(\mu_n^{(1)}(x_1,x_2)+\frac{1}{2\pi}I^{n,(1)}(x_1,x_2,k)\right)&=-2(f_{x_2}B^{(3)}+B^{(2)})\\
\sum_{n=0}^{\infty}\frac{1}{k^n}\left(\mu_n^{(2)}(x_1,x_2)+\frac{1}{2\pi}I^{n,(2)}(x_1,x_2,k)\right)&=\quad 2(f_{x_1}B^{(3)}+B^{(1)})
\end{aligned}\tag{13}$$

where the oscillatory integrals $I^{n,(l)}$ are defined as

$$\begin{aligned} I^{n,(l)}(x_1,x_2,k) =& ik\int_0^{2\pi} d\theta \int_0^{\infty} d\rho \ \exp\left[ik\Phi(x_1,x_2,\theta,\rho)\right] \\ & \times \left(H^{n,(l),(1)}(x_1,x_2,\theta,\rho) + H^{n,(l),(2)}(x_1,x_2,\theta,\rho) + F^{n,(l)}(x_1,x_2,\theta,\rho)\right) \\ & - \int_0^{2\pi} d\theta \int_0^{\infty} d\rho \ \exp\left[ik\Phi(x_1,x_2,\theta,\rho)\right] \\ & \times \left(K^{n,(l),(1)}(x_1,x_2,\theta,\rho) + K^{n,(l),(2)}(x_1,x_2,\theta,\rho) + G^{n,(l)}(x_1,x_2,\theta,\rho)\right) \end{aligned} \tag{14}$$

and where

$$\begin{aligned} \Phi(x_1,x_2,\theta,\rho) \ =& \ \rho\sin\theta\sin\psi\sin\phi - \cos\psi(f(x_1+\rho\cos\theta,x_2+\rho\sin\theta) - f(x_1,x_2)) \\ & + \rho\cos\theta\sin\psi\cos\phi + \left(\rho^2 + (f(x_1+\rho\cos\theta,x_2+\rho\sin\theta) - f(x_1,x_2))^2\right)^{1/2} \end{aligned}$$

and

$$\begin{aligned} F^{n,(l)}(x_1,x_2,\theta,\rho) &= \mu_n^{(l)}(x_1+\rho\cos\theta,x_2+\rho\sin\theta) \\ &\times\rho\frac{\rho\cos\theta f_{x_1}(x_1,x_2) + \rho\sin\theta f_{x_2}(x_1,x_2) + f(x_1,x_2) - f(x_1+\rho\cos\theta,x_2+\rho\sin\theta)}{\rho^2 + (f(x_1+\rho\cos\theta,x_2+\rho\sin\theta) - f(x_1,x_2))^2} \end{aligned}$$

$$\begin{aligned} G^{n,(l)}(x_1,x_2,\theta,\rho) &= \mu_n^{(l)}(x_1+\rho\cos\theta,x_2+\rho\sin\theta) \\ &\times\rho\frac{\rho\cos\theta f_{x_1}(x_1,x_2) + \rho\sin\theta f_{x_2}(x_1,x_2) + f(x_1,x_2) - f(x_1+\rho\cos\theta,x_2+\rho\sin\theta)}{(\rho^2 + (f(x_1+\rho\cos\theta,x_2+\rho\sin\theta) - f(x_1,x_2))^2)^{\frac{3}{2}}} \end{aligned}$$

$$\begin{aligned} H^{n,(l),(j)}(x_1,x_2,\theta,\rho) &= \mu_n^{(j)}(x_1+\rho\cos\theta,x_2+\rho\sin\theta) \\ &\times \frac{(f_{x_j}(x_1+\rho\cos\theta,x_2+\rho\sin\theta) - f_{x_j}(x_1,x_2))\rho^2\cos((l-1)\frac{\pi}{2}-\theta)}{\rho^2 + (f(x_1+\rho\cos\theta,x_2+\rho\sin\theta) - f(x_1,x_2))^2} \end{aligned}$$

$$\begin{aligned} K^{n,(l),(j)}(x_1,x_2,\theta,\rho) &= \mu_n^{(j)}(x_1+\rho\cos\theta,x_2+\rho\sin\theta) \\ &\times \frac{(f_{x_j}(x_1+\rho\cos\theta,x_2+\rho\sin\theta) - f_{x_j}(x_1,x_2))\rho^2\cos((l-1)\frac{\pi}{2}-\theta)}{(\rho^2 + (f(x_1+\rho\cos\theta,x_2+\rho\sin\theta) - f(x_1,x_2))^2)^{\frac{3}{2}}} \end{aligned}$$

for $1 \le j,l \le 2$.

As can be readily checked, the functions $F^{n,(l)}$, $G^{n,(l)}$, $H^{n,(j),(l)}$, $K^{n,(j),(l)}$, and Φ are smooth. Thus, it follows from the classical theory of oscillatory integrals [11] that the only significant contribution to the radial integrals in the definition of $I^{n,(l)}$ arises from the endpoint of integration $\rho = 0$ which, of course, corresponds to the target point in the original variables. In order to obtain the asymptotic expansion of $I^{n,(l)}$ we proceed by expanding each one of the integrands of $F^{n,(l)}$, $G^{n,(l)}$, $H^{n,(j),(l)}$, and $K^{n,(j),(l)}$ in Taylor series in powers of ρ around $\rho = 0$:

$$F^{n,(l)}(x_1,x_2,\theta,\rho) = \sum_{m=1}^{\infty} p_{n,m}^{(l)}(x_1,x_2,\theta)\rho^m, \quad 1 \le l \le 2, \tag{15}$$

$$G^{n,(l)}(x_1,x_2,\theta,\rho) = \sum_{m=0}^{\infty} q_{n,m}^{(l)}(x_1,x_2,\theta)\rho^m, \quad 1 \le l \le 2, \tag{16}$$

$$H^{n,(j),(l)}(x_1,x_2,\theta,\rho)=\sum_{m=1}^{\infty}h_{n,m}^{(j),(l)}(x_1,x_2,\theta)\rho^m,\quad 1\le j,l\le 2, \tag{17}$$

$$K^{n,(j),(l)}(x_1,x_2,\theta,\rho)=\sum_{m=0}^{\infty}k_{n,m}^{(j),(l)}(x_1,x_2,\theta)\rho^m,\quad 1\le j,l\le 2, \tag{18}$$

where we have used

$$p_{n,0}^{(l)}(x_1,x_2,\theta)=h_{n,0}^{(j),(l)}(x_1,x_2,\theta)=0,\quad 1\le j,l\le 2. \tag{19}$$

Next, expanding the phase Φ in a similar fashion

$$\Phi(x_1,x_2,\theta,\rho)=\Phi_1(x_1,x_2,\theta)\rho+\sum_{j=2}^{\infty}\Phi_j(x_1,x_2,\theta)\rho^j \tag{20}$$

and using (15)–(20) in (14) we obtain

$$\begin{aligned}I^{n,(l)}(x_1,x_2,k)=ik\sum_{m=1}^{\infty}&\int_0^{2\pi}\left(p_{n,m}^{(l)}(x_1,x_2,\theta)+h_{n,m}^{(l),(1)}(x_1,x_2,\theta)+h_{n,m}^{(l),(2)}(x_1,x_2,\theta)\right)d\theta\\&\times\int_0^{\infty}e^{ik\rho\Phi_1(x_1,x_2,\theta)}\left[e^{ik(\Phi(x_1,x_2,\theta,\rho)-\rho\Phi_1(x_1,x_2,\theta))}\right]\rho^m\,d\rho\\-\sum_{m=0}^{\infty}&\int_0^{2\pi}\left(q_{n,m}^{(l)}(x_1,x_2,\theta)+k_{n,m}^{(l),(1)}(x_1,x_2,\theta)+k_{n,m}^{(l),(2)}(x_1,x_2,\theta)\right)d\theta\\&\times\int_0^{\infty}e^{ik\rho\Phi_1(x_1,x_2,\theta)}\left[e^{ik(\Phi(x_1,x_2,\theta,\rho)-\rho\Phi_1(x_1,x_2,\theta))}\right]\rho^m\,d\rho.\end{aligned} \tag{21}$$

Finally, to allow for the *explicit* evaluation of the radial integral in $I^{n,(l)}(x_1,x_2,k)$, we expand the exponential in the bracketed expressions in the right-hand side of (21)

$$e^{ik(\Phi(x_1,x_2,\theta,\rho)-\Phi_1(x_1,x_2,\theta)\rho)}=1+\sum_{l\ge1}\frac{(k\rho)^l}{l!}\left(\sum_{j\ge l}a_{l,j}(x_1,x_2,\theta)\rho^j\right) \tag{22}$$

and we introduce the additional change of variables

$$t=k\rho$$

leading to

$$\begin{aligned}I^{n,(l)}(x_1,x_2,k)=\sum_{r=0}^{\infty}&\Big[\sum_{s=0}^{r}\sum_{j=0}^{s}\frac{i}{j!}\int_0^{2\pi}\Big(p_{n,1+r-s}^{(l)}(x_1,x_2,\theta)+h_{n,1+r-s}^{(l),(1)}(x_1,x_2,\theta)\\&+h_{n,1+r-s}^{(l),(2)}(x_1,x_2,\theta)\Big)a_{j,s}(x_1,x_2)A_0(1+r+j,x_1,x_2,\theta)\,d\theta\Big]k^{-r-1}\\-\sum_{r=0}^{\infty}&\Big[\sum_{s=0}^{r}\sum_{j=0}^{s}\frac{1}{j!}\int_0^{2\pi}\Big(q_{n,r-s}^{(l)}(x_1,x_2,\theta)+k_{n,r-s}^{(l),(1)}(x_1,x_2,\theta)\\&+k_{n,r-s}^{(l),(2)}(x_1,x_2,\theta)\Big)a_{j,s}(x_1,x_2)A_0(r+j,x_1,x_2,\theta)\,d\theta\Big]k^{-r-1}\end{aligned} \tag{23}$$

where

$$A_0(r,x_1,x_2,\theta) = \int_0^\infty e^{i\Phi_1(x_1,x_2,\theta)t} t^r\, dt = (\Phi_1(x,y,\theta))^{-r-1} \int_0^\infty e^{iv} v^r dv$$
$$= (\Phi_1(x,y,\theta))^{-r-1} e^{\frac{i\pi(r+1)}{2}} \Gamma(r+1) = \frac{r!\, e^{\frac{i\pi(r+1)}{2}}}{(\Phi_1(x,y,\theta))^{r+1}}. \tag{24}$$

We note here that, as in [7], the non-shadowing condition guarantees that the coefficient

$\Phi_1(x_1,x_2,\theta) = \sin\theta\sin\psi\sin\phi + \cos\theta\sin\psi\cos\phi$

$-\cos\psi(f_{x_1}(x_1,x_2)\cos\theta + f_{x_2}(x_1,x_2)\sin\theta) + \left(1 + (f_{x_1}(x_1,x_2)\cos\theta + f_{x_2}(x_1,x_2)\sin\theta)^2\right)^{1/2}$

defined in (20) does not vanish.

The explicit recurrence for the unknown coefficients $\mu_n^{(l)}$ now follows easily from (23) which shows, in particular, that

$$I^{n,(l)}(x_1,x_2,k) = O\left(\frac{1}{k}\right) \quad \text{as } k\to\infty.$$

Then, using (23) in (13) and equating like powers of k we have

$$\mu_0^{(1)}(x_1,x_2) = -2(f_{x_2}(x_1,x_2)B^{(3)} + B^{(2)}), \tag{25}$$

$$\mu_0^{(2)}(x_1,x_2) = \ \ 2(f_{x_1}(x_1,x_2)B^{(3)} + B^{(1)}), \tag{26}$$

and, for $n \geq 1$,

$$\begin{aligned}\mu_n^{(l)}(x_1,x_2) = -\frac{1}{2\pi}\sum_{m=0}^{n-1}\Big[\sum_{s=0}^{n-m-1}\sum_{j=0}^{s}\frac{i}{j!}\int_0^{2\pi}\Big(&p^{(l)}_{m,n-m-s}(x_1,x_2,\theta) + h^{(l),(1)}_{m,n-m-s}(x_1,x_2,\theta)\\ &+h^{(l),(2)}_{m,n-m-s}(x_1,x_2,\theta)\Big)\, a_{j,s}(x_1,x_2,\theta)A_0(n-m+j,x_1,x_2,\theta)\, d\theta\Big]\\ + \frac{1}{2\pi}\sum_{m=0}^{n-1}\Big[\sum_{s=0}^{n-m-1}\sum_{j=0}^{s}\frac{1}{j!}\int_0^{2\pi}\Big(&q^{(l)}_{m,n-m-s-1}(x_1,x_2,\theta) + k^{(l),(1)}_{m,n-m-s-1}(x_1,x_2,\theta)\\ &+k^{(l),(2)}_{m,n-m-s-1}(x_1,x_2,\theta)\Big)\, a_{j,s}(x_1,x_2,\theta)A_0(n-m+j-1,x_1,x_2,\theta)\, d\theta\Big].\end{aligned} \tag{27}$$

4. Numerical Experiments

4.1. Numerical implementation

The numerical implementation of the recurrence (25)–(27) follows the principles and the methods outlined in [7, Sec. 4]. In particular, the numerical algorithm is based on judicious manipulations of Taylor-Fourier series as described there. Again here, the overall simulation is divided into "pre-processing", "processing" and "postprocessing" stages. As in [7], the pre-processing stage is devoted to the precomputation of all quantities that depend only upon the geometry and incidence (e.g. $\Phi_j(x_1,x_2,\theta)$ and $a_{l,s}(x_1,x_2,\theta)$ defined in (20) and

(22), the integrals $A_0(r, x_1, x_2, \theta)$ in (24), etc); the processing stage, on the other hand, is the core of the scheme and where the recurrence (25)–(27) is actually implemented.

The pre-processing and processing steps deliver approximations to the current $\mathbf{J}$ via (8) and (12). From this, of course, all near- and far-field data can be recovered in a post-processing stage. In the important case of bi-periodic scattering surfaces, this data is encoded in a countable set of amplitudes, with only finitely many being relevant in the far-field. More precisely, the periodicity of the structure and the plane wave incidence imply the quasi-periodicity of the scattered fields which, on account of the "upoward-propagating" radiation conditions, can therefore be represented as [17]

$$\mathbf{E}(x_1, x_2, x_3) = \sum_{r=-\infty}^{\infty} \sum_{s=-\infty}^{\infty} \mathbf{B}_{r,s} \exp(i\alpha_r x_1 + i\beta_s x_2 + i\gamma_{r,s} x_3)\,, \quad x_3 > \max f(x_1, x_2)\,, \tag{28}$$

and similarly for $\mathbf{H}$. Here

$$\alpha_r = \alpha + \frac{2\pi r}{d_1}, \quad \beta_s = \beta + \frac{2\pi s}{d_1}, \quad \text{and} \quad \gamma_{r,s} = \left(k^2 - \alpha_r^2 - \beta_s^2\right)^{1/2}$$

where the square root is chosen so that $\Im(\gamma_{r,s}) \geq 0$; the finitely many propagating modes, i.e. those that do not decay in the far-field, correspond to the indices in the (finite) set $U = \{(r, s) : \Im(\gamma_{r,s}) = 0\}$.

Explicit formulas for the coefficients $\mathbf{B}_{r,s}$ in (28) can be derived in terms of the computed approximation to $\mathbf{J}_{\text{slow}}$. Indeed, using the periodized Green's function

$$G_k^{\text{per}}(x_1, x_2, x_3) = \frac{i}{2d_1 d_2} \sum_{r=-\infty}^{\infty} \sum_{s=-\infty}^{\infty} \frac{1}{\gamma_{r,s}} e^{i\alpha_r x_1 + i\beta_s x_2 + i\gamma_{r,s}|x_3|}.$$

and the formula

$$\nabla_{\mathbf{x}}^t \cdot \mathbf{J}(\mathbf{x}) = \frac{1}{\sqrt{g}} \left(\frac{\partial}{\partial x_1}(J^{(1)}(x_1, x_2)\sqrt{g}) + \frac{\partial}{\partial x_2}(J^{(2)}(x_1, x_2)\sqrt{g}) \right)$$

in (5) an integration by parts readily yields

$$\begin{aligned}
B_{r,s}^{(1)} &= -\frac{k}{2\gamma_{r,s}} I_{r,s}^{1,1} - \frac{i\alpha_r}{2k\gamma_{r,s}} \left(i\alpha_r I_{r,s}^{1,1} + i\gamma_{r,s} I_{r,s}^{1,2} \right) - \frac{i\alpha_r}{2k\gamma_{r,s}} \left(i\beta_s I_{r,s}^{2,1} + i\gamma_{r,s} I_{r,s}^{2,2} \right) \\
B_{r,s}^{(2)} &= -\frac{k}{2\gamma_{r,s}} I_{r,s}^{2,1} - \frac{i\beta_s}{2k\gamma_{r,s}} \left(i\alpha_r I_{r,s}^{1,1} + i\gamma_{r,s} I_{r,s}^{1,2} \right) - \frac{i\beta_s}{2k\gamma_{r,s}} \left(i\beta_s I_{r,s}^{2,1} + i\gamma_{r,s} I_{r,s}^{2,2} \right) \\
B_{r,s}^{(3)} &= -\frac{\alpha_r B_{r,s}^{(1)} + \beta_s B_{r,s}^{(2)}}{\gamma_{r,s}}
\end{aligned}$$

where

$$\begin{aligned}
I_{r,s}^{l,j} = \frac{1}{d_1 d_2} \int_0^{d_1} \int_0^{d_2} \exp &\left[-i\frac{2\pi r}{d_1} x_1 - i\frac{2\pi s}{d_2} x_2 - i(\gamma_{r,s} + \gamma) f(x_1, x_2) \right] \\
&\times ((j-1) f_{x_l}(x_1, x_2) + \delta_j^1) J_{\text{slow}}^{(l)}(x_1, x_2) \sqrt{g}\, dx_1 dx_2
\end{aligned}$$

with $1 \leq j, l \leq 2$ and $(r, s) \in U$. In the next section we shall present some examples of evaluation of these quantities for a variety of surfaces and illuminations. In addition to the

computed values of some specific and representative amplitudes we shall also include that of the "defect" in energy conservation which, for any given approximation, is defined as

$$\epsilon = \left| 1 - \sum_{(r,s)\in U} e_{r,s} \right| \tag{29}$$

where the *efficiency* $e_{r,s}$ is given by

$$e_{r,s} = \frac{|\mathbf{B}_{r,s}|^2 \gamma_{r,s}}{|\mathbf{A}|^2 \gamma_{0,0}}.$$

4.2. Numerical results

In this section, we present numerical results obtained from the implementation of the recurrence (25)-(27) for several profiles and incidences. To facilitate the comparision with the acoustic case, we shall consider examples for the same profiles as used in [7]. To recall, these included a "bisinusoidal" structure

$$f_1(x,y) = \frac{h}{h_1}(\cos(2\pi x) + \cos(2\pi y)), \tag{30}$$

a more oscillatory one of the form

$$f_2(x,y) = \frac{h}{h_2}(\cos(2\pi x) + \cos(4\pi x) + \cos(2\pi y) + \cos(4\pi y)) \tag{31}$$

and, finally, a rougher surface defined as

$$f(x,y) = \frac{h}{h_3}(\cos(2\pi x) + \frac{1}{4}\cos(4\pi x) + \frac{1}{6}\sin(6\pi x))(\cos(2\pi y) + \cos(4\pi y)). \tag{32}$$

Here $h_1 = 4$, $h_2 \approx 6.24$ and $h_3 \approx 4.4$ are chosen so that the value of h remains indicative of the height of the profile.

The first set of results, Tables 1–12, correspond to scattering experiments for the three profiles above with a height $h = 0.015$ and illuminated with a wavelength $\lambda = 0.021$. For each profile, we display results corresponding to two orthogonal polarizations in normal (Tables 1–6) and off-normal incidence (Tables 7–12). Each table shows the relative errors incurred by our approximations, up to order ten, in the same illustrative efficiencies chosen in [7], along with the corresponding energy defects (29). The "exact" results were computed with an alternative scheme, the "Method of Variation of Boundaries" [24], that is known to be highly accurate in the "resonance regime" $h \approx \lambda$. (The slight difference in the wavelength chosen here —$\lambda = 0.021$— as compared to that in Tables 1–3 and 5–7 of [7] —$\lambda = 0.020$— is due to the need of the exact solver of [24] to remain away from anomalous —"Wood"— frequencies in the vector electromagnetic case). The results in these tables show essentially no deterioration in their quality when compared to those obtained in the scalar case (cf. Tables 1–3 and 5–7 of [7]): again here the algorithm converges rapidly even for configurations in this resonance region, where it can readily provide results with up to full double-precision accuracy at a very modest computational cost.

Table 1. Results for the profile (30) with $\lambda = 0.021$, $\mathbf{A} = (1, 0, 0)$, $\psi = 0^o$, $\phi = 0^o$.

Efficiency	Scattered energy	Order 0	Order 1	Order 3	Order 5	Order 10
(0,0)	0.5481713774436903e-04	9.51e-06	9.51e-06	4.39e-10	5.48e-12	2.20e-13
(1,0)	0.2248926107565851e-02	3.00e-03	1.46e-06	1.81e-09	2.25e-12	8.87e-15
(1,1)	0.9115901959623925e-01	1.85e-07	1.36e-07	2.53e-10	4.55e-13	3.65e-15
(1,2)	0.4916096425663652e-01	3.75e-04	2.50e-07	3.97e-10	6.40e-13	1.27e-15
(2,2)	0.2647205147564099e-01	1.56e-07	3.86e-08	1.18e-10	2.31e-13	2.62e-15
(2,4)	0.4176404049747460e-03	5.35e-04	1.08e-06	1.08e-09	1.21e-12	2.59e-16
ϵ	1.18e-15	6.12e-08	4.90e-14	2.46e-16	4.36e-17	8.84e-18

Table 2. Results for the profile (31) with $\lambda = 0.021$, $\mathbf{A} = (1, 0, 0)$, $\psi = 0^o$, $\phi = 0^o$.

Efficiency	Scattered energy	Order 0	Order 1	Order 3	Order 5	Order 10
(0,0)	0.2052506267805416e-01	6.64e-07	6.64e-07	2.80e-09	1.56e-11	5.74e-15
(1,0)	0.2440734151214156e-01	2.85e-04	2.46e-06	5.25e-09	8.95e-12	2.84e-15
(1,1)	0.2899700677756021e-01	5.71e-07	3.56e-07	1.55e-09	3.39e-12	1.31e-14
(1,2)	0.1672732578486777e-01	3.57e-04	8.01e-07	8.64e-10	1.50e-11	1.07e-14
(2,2)	0.9666148668162721e-02	1.14e-06	4.58e-07	8.87e-09	6.89e-11	2.87e-15
(2,4)	0.2377203874010919e-02	9.50e-04	2.50e-06	1.57e-08	9.79e-11	1.62e-14
ϵ	2.54e-15	4.26e-07	2.93e-12	1.90e-15	1.65e-15	7.95e-16

Table 3. Results for the profile (32) with $\lambda = 0.021$, $\mathbf{A} = (1, 0, 0)$, $\psi = 0^o$, $\phi = 0^o$.

Efficiency	Scattered energy	Order 0	Order 1	Order 3	Order 5	Order 10
(0,0)	0.1446642494690797e-00	4.88e-04	1.78e-06	4.65e-09	1.62e-11	1.91e-15
(1,0)	0.2867209658663495e-01	2.27e-04	1.94e-06	3.54e-08	1.18e-09	1.96e-13
(1,1)	0.2363063135982192e-01	1.29e-03	2.32e-06	4.35e-08	1.11e-09	1.69e-13
(1,2)	0.1965546006015095e-01	2.51e-04	1.66e-07	2.62e-08	8.19e-10	1.18e-13
(2,2)	0.1545490252505550e-02	1.09e-03	5.60e-06	9.06e-08	4.24e-09	6.89e-13
(2,4)	0.1739945943990244e-04	1.86e-03	5.69e-05	1.44e-06	4.32e-08	8.05e-12
ϵ	1.64e-16	6.66e-07	3.27e-11	1.03e-14	1.41e-15	1.52e-15

Table 4. Results for the profile (30) with $\lambda = 0.021$, $\mathbf{A} = (0, 1, 0)$, $\psi = 0^o$, $\phi = 0^o$.

Efficiency	Scattered energy	Order 0	Order 1	Order 3	Order 5	Order 10
(0,0)	0.5481713774436163e-04	9.51e-06	9.51e-06	4.39e-10	5.34e-12	3.55e-13
(1,0)	0.2235427945333268e-02	3.01e-03	9.01e-07	4.13e-09	7.71e-12	2.85e-14
(1,1)	0.9115901959623986e-01	1.85e-07	1.36e-07	2.53e-10	4.48e-13	2.89e-15
(1,2)	0.4919791353700149e-01	3.75e-04	2.93e-07	3.09e-10	4.22e-13	2.53e-15
(2,2)	0.2647205147564092e-01	1.56e-07	3.86e-08	1.18e-10	2.28e-13	3.93e-16
(2,4)	0.4180877804685924e-03	5.35e-04	1.96e-06	3.89e-09	6.76e-12	1.12e-14
ϵ	8.71e-17	6.12e-08	4.91e-14	2.32e-16	2.64e-17	2.55e-16

Table 5. Results for the profile (31) with $\lambda = 0.021$, $\mathbf{A} = (0, 1, 0)$, $\psi = 0^o$, $\phi = 0^o$.

Efficiency	Scattered energy	Order 0	Order 1	Order 3	Order 5	Order 10
(0,0)	0.2052506267805453e-01	6.64e-07	6.64e-07	2.80e-09	1.57e-11	1.21e-14
(1,0)	0.2439337687208378e-01	2.87e-04	7.40e-07	2.36e-09	2.00e-11	1.13e-15
(1,1)	0.2899700677756055e-01	5.71e-07	3.56e-07	1.55e-09	3.38e-12	1.43e-15
(1,2)	0.1673922906892367e-01	3.54e-04	1.69e-06	1.36e-08	8.80e-11	4.76e-15
(2,2)	0.9666148668162667e-02	1.14e-06	4.58e-07	8.87e-09	6.89e-11	8.43e-15
(2,4)	0.2381718126941798e-02	9.46e-04	3.63e-06	1.33e-08	6.28e-11	1.63e-14
ϵ	1.47e-15	4.27e-07	2.93e-12	2.10e-15	1.72e-15	5.20e-16

Table 6. Results for the profile (32) with $\lambda = 0.021$, $\mathbf{A} = (0, 1, 0)$, $\psi = 0^o$, $\phi = 0^o$.

Efficiency	Scattered energy	Order 0	Order 1	Order 3	Order 5	Order 10
(0,0)	0.1445225220891838e-00	4.91e-04	9.78e-07	1.83e-09	3.16e-12	4.22e-15
(1,0)	0.2868514579308918e-01	2.27e-04	2.70e-06	3.03e-08	3.14e-10	1.31e-14
(1,1)	0.2356937116427616e-01	1.29e-03	4.82e-07	3.07e-08	3.77e-10	9.71e-15
(1,2)	0.1966536999082089e-01	2.52e-04	9.99e-07	8.19e-09	3.65e-12	2.69e-14
(2,2)	0.1548890608904114e-02	1.10e-03	1.84e-06	1.09e-08	5.60e-12	5.29e-14
(2,4)	0.1734004455343712e-04	1.55e-03	3.31e-05	3.32e-07	3.58e-09	3.67e-13
ϵ	7.65e-16	6.67e-07	1.54e-11	3.40e-15	1.21e-15	7.07e-16

As in [7], we further illustrate the significant improvement in accuracy as the order of the expansion is increased with an example spanning a broad portion of the electromagnetic spectrum. Specifically, in Figure 1 we present the error in the efficiency $e_{0,0}$ as a function of

Table 7. Results for the profile (30) with $\lambda = 0.021$, V polarization, $\psi = 30^o$, $\phi = 10^o$.

Efficiency	Scattered energy	Order 0	Order 1	Order 3	Order 5	Order 10
(0,0)	0.4336864443245527e-02	4.32e-04	7.82e-07	2.02e-08	1.55e-10	9.19e-15
(1,0)	0.2361649908761896e-01	1.12e-03	9.52e-06	9.96e-09	6.48e-12	8.96e-15
(1,1)	0.1135234005657680e-00	1.30e-05	1.00e-05	1.08e-08	8.22e-12	1.83e-15
(1,2)	0.3795478216233337e-01	4.16e-04	9.96e-06	1.06e-08	9.49e-12	5.30e-15
(2,2)	0.1218682441785825e-01	1.53e-04	2.31e-05	4.19e-08	7.91e-11	4.98e-15
(2,4)	0.8763485621371705e-04	4.98e-04	2.17e-05	4.19e-08	8.92e-11	5.87e-15
ϵ	4.49e-17	1.13e-07	5.40e-11	1.36e-15	9.52e-16	1.05e-15

Table 8. Results for the profile (31) with $\lambda = 0.021$, V polarization, $\psi = 30^o$, $\phi = 10^o$.

Efficiency	Scattered energy	Order 0	Order 1	Order 3	Order 5	Order 10
(0,0)	0.4229547562014422e-01	3.58e-04	5.16e-07	9.99e-08	2.62e-09	3.12e-13
(1,0)	0.3585723269920608e-01	5.87e-04	3.05e-05	1.77e-07	1.70e-09	3.30e-13
(1,1)	0.2916958261008928e-01	1.16e-04	3.37e-05	1.79e-07	1.58e-09	2.93e-13
(1,2)	0.2022684051277380e-01	7.10e-04	3.36e-05	1.91e-07	1.69e-09	3.12e-13
(2,2)	0.1419200390550528e-01	1.21e-04	7.57e-05	2.71e-07	1.84e-09	1.09e-13
(2,4)	0.2013375199931759e-02	1.07e-03	7.32e-05	2.69e-07	2.02e-09	9.58e-14
ϵ	1.60e-16	7.29e-07	1.47e-09	8.51e-14	2.82e-17	1.22e-15

Table 9. Results for the profile (32) with $\lambda = 0.021$, V polarization, $\psi = 30^o$, $\phi = 10^o$.

Efficiency	Scattered energy	Order 0	Order 1	Order 3	Order 5	Order 10
(0,0)	0.2170109037942736e-00	3.62e-04	1.79e-05	7.26e-07	3.37e-08	2.13e-10
(1,0)	0.2162615791322058e-01	2.88e-04	3.61e-06	7.79e-07	3.48e-09	2.20e-10
(1,1)	0.3023785286886791e-01	1.58e-03	2.94e-05	3.53e-07	1.04e-08	8.89e-11
(1,2)	0.2764992080850899e-01	3.43e-04	2.74e-05	2.44e-07	4.05e-08	1.10e-10
(2,2)	0.4735126162788356e-03	3.83e-03	6.09e-04	1.73e-05	2.29e-07	4.83e-10
(2,4)	0.2901388517501337e-03	3.60e-05	9.09e-06	4.99e-06	5.30e-08	2.79e-10
ϵ	9.79e-16	1.23e-06	9.67e-09	2.01e-11	1.49e-13	1.57e-14

Table 10. Results for the profile (30) with $\lambda = 0.021$, H polarization, $\psi = 30^o$, $\phi = 10^o$.

Efficiency	Scattered energy	Order 0	Order 1	Order 3	Order 5	Order 10
(0,0)	0.4340596526413628e-02	4.27e-04	2.33e-06	4.11e-09	1.99e-11	3.59e-15
(1,0)	0.2356342951047420e-01	1.12e-03	4.57e-06	2.25e-10	7.71e-12	8.39e-15
(1,1)	0.1135262912050163e-00	1.24e-05	4.45e-06	2.06e-09	1.52e-12	2.68e-15
(1,2)	0.3798636443739307e-01	4.15e-04	3.09e-06	4.69e-10	6.19e-12	1.46e-15
(2,2)	0.1218306587190246e-01	1.54e-04	9.86e-06	7.53e-09	8.25e-12	4.84e-15
(2,4)	0.8772227631289198e-04	4.98e-04	5.22e-06	5.35e-09	3.22e-11	6.33e-15
ϵ	7.58e-16	1.13e-07	2.26e-11	6.63e-16	9.97e-16	6.57e-16

Table 11. Results for the profile (31) with $\lambda = 0.021$, H polarization, $\psi = 30^o$, $\phi = 10^o$.

Efficiency	Scattered energy	Order 0	Order 1	Order 3	Order 5	Order 10
(0,0)	0.4232570470333260e-01	3.56e-04	9.12e-07	1.78e-08	3.72e-10	3.65e-14
(1,0)	0.3581494616159046e-01	5.92e-04	1.69e-05	3.21e-08	1.34e-10	3.08e-14
(1,1)	0.2917633091088374e-01	1.14e-04	1.45e-05	3.28e-08	2.37e-10	3.15e-14
(1,2)	0.2025550588151870e-01	7.05e-04	1.33e-05	4.15e-08	3.99e-10	3.75e-14
(2,2)	0.1418848397276147e-01	1.26e-04	3.31e-05	5.21e-08	2.95e-10	3.72e-14
(2,4)	0.2017689031030438e-02	1.06e-03	2.03e-05	5.27e-08	1.15e-09	6.36e-14
ϵ	1.70e-15	7.29e-07	6.18e-10	9.89e-15	6.63e-16	4.84e-16

Table 12. Results for the profile (32) with $\lambda = 0.021$, H polarization, $\psi = 30^o$, $\phi = 10^o$.

Efficiency	Scattered energy	Order 0	Order 1	Order 3	Order 5	Order 10
(0,0)	0.2168524774056718e-00	3.67e-04	5.21e-06	1.27e-07	3.13e-09	1.51e-11
(1,0)	0.2163867201690774e-01	2.89e-04	8.52e-06	1.71e-07	9.98e-10	1.11e-11
(1,1)	0.3014199854789860e-01	1.59e-03	1.99e-05	7.13e-08	3.72e-09	4.35e-12
(1,2)	0.2763092444554548e-01	3.44e-04	1.22e-05	2.78e-07	8.41e-09	9.16e-12
(2,2)	0.4699008279945933e-03	3.81e-03	2.35e-04	3.31e-06	1.75e-08	5.59e-11
(2,4)	0.2901776163762193e-03	9.75e-05	1.40e-04	2.50e-06	1.06e-08	7.54e-11
ϵ	2.05e-15	1.23e-06	4.62e-09	3.33e-12	9.44e-15	6.96e-15

the wavelength of radiation for a configuration with off-normal incidence ($\psi = 30^o$, $\phi = 10^o$) on the profile (30) with $h = 0.025$. In these plots the wavelength covers several orders of magnitude, from the very high-frequency ($\lambda = 2 \times 10^{-6}$) to the resonance ($\lambda \approx h$) to the low frequency ($\lambda = 0.135$) regimes. The figures show that very high precision can be attained throughout by increasing the order of the expansion in (12) (here, for short wavelengths, below resonance, the reference solution was taken to be that produced by our new scheme at order 20).

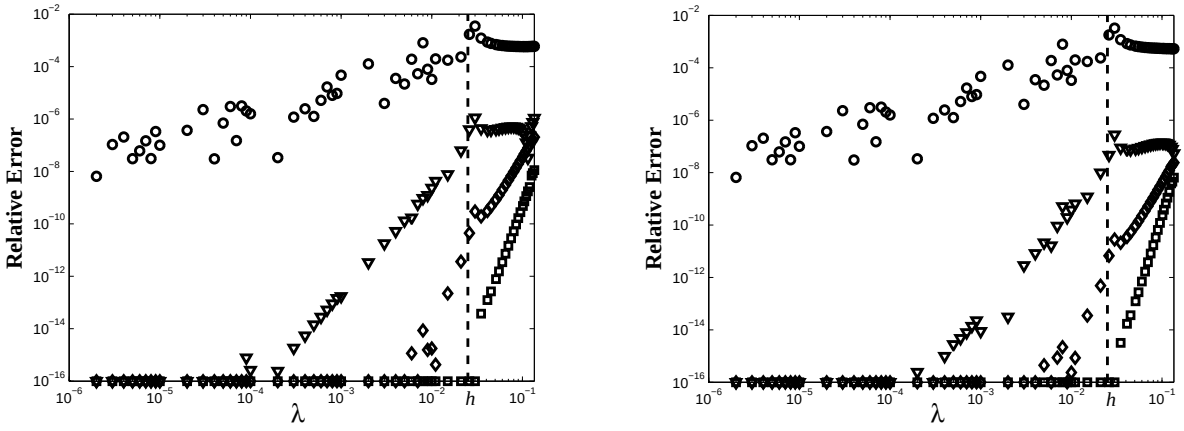

(a) V polarization

(b) H polarization

Figure 1. Relative errors in the prediction of the efficiency of order $(0, 0)$ for the profile (30) with $h = 0.025$ under normal incidence as a function of the wavelength of radiation. Comparison of results for asymptotic expansions of orders 0 (Kirchhoff, circles), 3 (triangles), 7 (diamonds) and 12 (squares).

We conclude with two examples where the incidence azimuthal angle ψ is near to grazing. In Tables 13 and 14 we display results corresponding to the bisinusoidal profile with $h = 0.01$, $\lambda = 0.0002$ and $\psi = 80^o$, in the vertical and horizontal polarizations respectively. Again here, the results show a significant improvement with increasing order, converging at the same rate as in the acoustic case (compare with Table 8 of [7]).

5. Conclusions

We have presented a new numerical scheme for the simulation of fully three-dimensional electromagnetic rough-surface scattering problems. The method allows for the accurate evaluation of scattered fields from low to high frequencies at a cost that is independent of the wavelength of radiation. The procedure extends the ideas and techniques introduced in the first paper of this series [7] to the vector electromagnetic case, and it is based on a *high-order* asymptotic evaluation of the solution of an integral equation formulation of the

Table 13. Results for the profile (30) with $\lambda = 0.0002$, $h = 0.01$, V polarization, $\psi = 80^o$, $\phi = 0^o$.

Efficiency	Scattered energy	Order 0	Order 1	Order 3	Order 5	Order 7
(0,0)	0.1165361086639181e-05	2.65e-03	2.30e-06	1.86e-09	1.61e-12	1.01e-14
(1,0)	0.4586696609463535e-04	2.24e-04	2.61e-06	2.40e-09	2.09e-13	0.00e-00
(1,1)	0.4639891990588888e-03	1.61e-04	2.62e-06	2.40e-09	1.97e-13	7.94e-15
(1,2)	0.2692220871081306e-04	2.43e-04	2.60e-06	2.40e-09	1.96e-13	8.43e-15
(2,2)	0.5594124340429963e-05	1.78e-03	1.89e-06	2.10e-09	1.60e-12	9.53e-15
(2,4)	0.5702729507995484e-06	1.66e-03	2.12e-06	2.08e-09	1.64e-12	0.00e-00
ϵ	4.66e-15	4.64e-08	9.38e-12	3.88e-15	4.44e-15	4.00e-15

Table 14. Results for the profile (30) with $\lambda = 0.0002$, $h = 0.01$, H polarization, $\psi = 80^o$, $\phi = 0^o$.

Efficiency	Scattered energy	Order 0	Order 1	Order 3	Order 5	Order 7
(0,0)	0.1171559400758398e-05	2.64e-03	1.06e-06	4.97e-10	2.90e-13	5.06e-15
(1,0)	0.4584634382487682e-04	2.25e-04	1.30e-06	6.49e-10	1.64e-14	1.62e-15
(1,1)	0.4638388126154015e-03	1.62e-04	1.30e-06	6.49e-10	1.54e-14	1.40e-15
(1,2)	0.2690908255242728e-04	2.44e-04	1.30e-06	6.49e-10	1.59e-14	1.63e-15
(2,2)	0.5614117868899808e-05	1.78e-03	9.17e-07	5.67e-10	2.78e-13	3.01e-15
(2,4)	0.5721690805569265e-06	1.65e-03	9.11e-07	5.72e-10	2.89e-13	4.99e-15
ϵ	2.33e-15	4.64e-08	2.34e-12	2.77e-15	2.55e-15	2.33e-15

scattering problem. We have shown that, in spite of the considerably more involved nature of the derivations and resulting formulas, the performance of the method retains the favorable characteristics that were demonstrated in the treatment of acoustic scattering problems. In particular, results with full double-precision accuracy were presented for various geometries, incidences and polarizations. As we demonstrated, these results constitute very significant improvements over alternative low-order theories (e.g. the Kirchhoff approximation), and they are attainable at a modest additional computational cost. As in these alternative theories, our current implementation is restricted to non-shadowing configurations where the scatter results from direct incidence. Extensions to shadowing/multiple-scattering geometrical arrangements will be the subject of future work.

Acknowledgments

Fernando Reitich gratefully acknowledges support from AFOSR through contract No. FA9550-05-1-0019, from NSF through grant No. DMS–0311763, and from the Army High Performance Computing Research Center (AHPCRC) under Army Research Laboratory cooperative agreement number DAAD19-01-2-0014.

Disclaimer. Effort sponsored by the Air Force Office of Scientific Research, Air Force Materials Command, USAF, under grant number FA9550-05-1-0019, and by AHPCRC under the auspices of the Department of the Army, Army Research Laboratory cooperative agreement number DAAD19-01-2-0014. The US Government is authorized to reproduce and distribute reprints for governmental purposes notwithstanding any copyright notation thereon. The views and conclusions contained herein are those of the author and should not be interpreted as necessarily representing the official policies or endorsements, either expressed or implied, of the Air Force Office of Scientific Research, the Army Research Laboratory or the US Government.

References

[1] Beckmann P and Spizzichino A 1963 *The Scattering of Electromagnetic Waves from Rough Surfaces: Part I. Theory* (London: Pergamon)

[2] Ogilvy J A 1991 *Theory of Wave Scattering from Random Rough Surfaces* (Bristol: Adam Hilger)

[3] Lynch P J 1970 Curvature corrections to rough-surface scattering at high frequencies *J. Acoust. Soc. Am.* **47** 804–815

[4] Liszka E G and McCoy J J 1982 Scattering at a rough boundary —Extensions of the Kirchhoff approximation *J. Acoust. Soc. Am.* **71** 1093–1100

[5] Chaloupka H and Meckelburg H 1985 Improved high-frequency current approximation for curved conducting surfaces *Arch. Elektron. bertragungstech.* **39** 245–250

[6] Rodriguez E 1991 Beyond the Kirchhoff approximation II electromagnetic scattering *Radio Sci.* **26** 121–132

[7] Reitich F and Turc C 2004 High-order solutions of three-dimensional rough-surface scattering problems at high-frequencies. I: the scalar case *Waves Random Media* to appear

[8] Bruno O, Sei A and Caponi M 2002 High-order high-frequency solutions of rough surface scattering problems *Radio Sci.*

[9] Hsiao G. C. and Kleinman R E. 1997 Mathematical foundations for error estimation in numerical solutions of integral equations in electromagnetics *IEEE Trans. Antennas Propag.* **45** 316–328 **37** 2/1-2/13

[10] Maue A W 1949 On the formulation of a general scattering problem by means of an integral equation *Z. Phys.* **125** 601-18

[11] Bleistein N and Handelsman R A 1986 *Asymptotic Expansions of Integrals* (New York: Dover)

[12] Bruce N C 2004 On the validity of the inclusion of geometrical shadowing functions in the multiple-scatter Kirchhoff approximation *Waves Random Media* **14** 1–12

[13] Bouche D, Molinet F and Mittra R 1997 *Asymptotic Methods in Electromagnetics* (New York: Springer-Verlag)

[14] Bruno O P, Geuzaine C A, Monroe J A and Reitich F 2004 Prescribed error tolerances within fixed

computational times for scattering problems of arbitrarily high frequency: the convex case *Phil. Trans. Roy. Soc. London* **362** 629–45

[15] Colton D, and Kress R 1992 *Inverse Acoustic and Electromagnetic Scattering Theory* (New York, Springer Verlag)

[16] Chandler-Wilde S N and Zhang B 1998 Electromagnetic scattering by an inhomogeneous conducting or dielectric layer on a perfectly conducting plate *Proc. Royal Soc. London Ser. A* **454** 519–42

[17] Petit R. 1980 A tutorial introduction *Electromagnetic Theory of Gratings* (New York: Springer-Verlag) 1–40

[18] Stratton J A and Chu L J 1939 Diffraction theory of electromagnetic waves *Phys. Rev.* **56** 99–107

[19] Cullen J A 1958 Surface currents induced by short-wavelength radiation, *Phys. Rev. B*, **109**, 1863–1867

[20] Fock V 1965 Electromagnetic diffraction and propagation problems (London: Pergamon Press) 3–22, 1863–1867

[21] Melrose R and Taylor M 1985 Near peak scattering and the correct Kirchhoff approximation for a convex obstacle *Adv. in Math.* **55** 242–315

[22] Voronovich A G 1994 *Wave Scattering from Rough Surfaces* (New York: Springer-Verlag)

[23] Charnotskii M I and Tatarskii V I 1995 Tilt-invariant theory of rough-surface scattering: I *Waves Random Media* **5** 361–380

[24] Bruno O P and Reitich F 1993 Numerical solution of diffraction problems: a method of variation of boundaries. III. Doubly periodic gratings *Journal Opt. Soc. Am. A* **10** 2551–2562